Transglutaminase-2 of pancreatic cancer cells assembles a CXCL12-keratin 19-coat that mediates the resistance to immunotherapy

Zhikai Wang[1], Jiayun Li[1], Ya Gao[1], Tobias Janowitz[1,2], and Douglas Fearon[1,3*].

Affiliations:

[1]Cold Spring Harbor Laboratory, Cold Spring Harbor, NY 11724

[2]Northwell Health, New York, NY 11021

[3]Weill Cornell Medicine, New York, NY 10065

[*]Correspondence to:
Douglas T. Fearon
Cold Spring Harbor Laboratory
1 Bungtown Road
Cold Spring Harbor, NY 11724, USA
Phone: 516 367 5420
Email: dfearon@cshl.edu

Abstract: To enhance efficacy of cancer immunotherapy, we must discover how adenocarcinomas resist PD-1-directed therapy. In a mouse model of pancreatic ductal adenocarcinoma (PDA), it has been shown that inhibiting the chemokine receptor, CXCR4, overcomes resistance to anti-PD-L1. Here, we show that the PDA cancer cells exhibit an extracellular, covalent complex between keratin 19 (KRT19) and CXCL12, the ligand for CXCR4, which is produced by the cancer-associated fibroblast (CAF). PDA tumors containing gene-edited cancer cells that cannot express KRT19 or transglutaminase-2 (TGM2) lack the CXCL12-coat, are infiltrated with T cells, and regress during treatment of tumor-bearing mice with anti-PD-1. Therefore, TGM2 of pancreatic cancer cells enables their escape from immune attack by capturing the immune suppressive chemokine of the CAF. These findings may explain the resistance to immunotherapy of multiple human adenocarcinomas in which we find this CXCL12-coat.

One Sentence Summary: Gene editing murine pancreatic cancer cells to prevent their CXCL12-coat assembly enables T cell-directed immunotherapy to eliminate tumors.

Main Text:

The resistance of most solid tumors to inhibitors of the PD-1 checkpoint is the major problem in cancer immunology, and a relative absence of T cells in nests of adenocarcinoma cells correlates with this resistance (*1, 2*). Several explanations for this impaired accumulation of intra-tumoral T cells have been proposed, including poor immunogenicity of the cancer cells (*3-5*), immune suppressive enzymes and cytokines (*6, 7*), exhaustion of intra-tumoral T cells (*8*), and the presence of immune suppressive cell types (*9*), but therapeutic approaches based on these explanations has not been successful.

The trafficking of immune cells into and within tissues is regulated by their chemokine receptors responding to chemokines produced at these sites. The complexity of this system, which includes more than 50 chemokines and chemokine receptors, enables the assembly of the different populations of immune cells that can mediate the diversity of responses that characterize the immune system (*10*). A relevant interaction between the cancer cell and this chemokine/chemokine receptor system was suggested by the finding that CXCL12, which is produced by CAFs (*11, 12*), appeared to "coat" cancer cells in a mouse model of PDA (*13*). Moreover, CXCL12 was shown to mediate tumoral immune suppression in mouse PDA when conditionally depleting CAFs or inhibiting CXCR4, the CXCL12 receptor, increased T cell infiltration, controlled tumor growth, and uncovered sensitivity to inhibition of the PD-1 checkpoint (*13, 14*). Here, we examine how mouse PDA cancer cells capture CXCL12 and the role of the resulting CXCL12-coat in suppressing the intra-tumoral trafficking of T cells and the anti-tumor effects of anti-PD-1 therapy.

We assessed whether the finding of the CXCL12-coat in mouse PDA was relevant to human cancer. Fluorescently labeled anti-CXCL12 antibodies stained the KRT19-expressing cells in sections of human pancreatic, colon, breast, and bladder cancers, respectively (Fig. 1A), all tumors that have been reported to exclude T cells, and other KRT19-expressing adenocarcinomas that resist PD-1-directed immunotherapy (*15, 16*) (Fig. S1A). Melanoma cells, which do not express KRT19, are not coated with CXCL12 (Fig. S1A). The KRT19-expressing cancer cells in mouse autochthonous and subcutaneous PDA tumors were also stained with anti-CXCL12 antibody, and T cells were seen in the stromal regions of the tumors but not in cancer cell nests (Fig. 1B, C). *Cxcl12* mRNA was detected in the PDGFRα-expressing, fibroblastic stromal cells by fluorescent in situ hybridization (FISH), but not in the KRT19-expressing cancer cells of these tumors (Fig. S1B), demonstrating that the cancer cell-associated CXCL12 was derived from the CAFs. Confocal microscopy of individual PDA cells that were not permeabilized in mouse tumors showed co-localization of CXCL12 and KRT19 to the periphery of the cells (Fig. 1D). We confirmed the extracellular location of KRT19 and CXCL12 by FACS analysis of intact cancer cells released from subcutaneous PDA tumors that had been stained with anti-KRT19 and anti-CXCL12 antibodies (Fig. S1C).

To examine further the association of CXCL12 with the PDA cells, we excised subcutaneous PDA tumors, treated them sequentially with NP-40, sodium deoxycholate (DOC), DNase, and sodium dodecyl sulfate (SDS), and analyzed the lysates by SDS-polyacrylamide gel electrophoresis (SDS-PAGE) and immunoblotting with anti-KRT19 and anti-CXCL12 antibodies. CXCL12 was detected only in the tumor lysate obtained with SDS, with an apparent molecular weight of ~52 kD, instead of its native molecular weight of 9-11 kD (Fig. 1E). KRT19 also was released by SDS-treatment of the PDA tumors, with the major band having the ~44 kD molecular weight of the native protein and two minor bands with higher apparent molecular weight. We assessed the possibility that the high molecular weight forms of CXCL12 and KRT19 represented a complex by subjecting the SDS-lysate to immunoprecipitation with anti-CXCL12 antibody, and analyzing the precipitated proteins by SDS-PAGE followed by immunoblotting. A single band was detected with anti-KRT19 antibody that co-migrated with the high molecular weight form of CXCL12 (Fig. 1F), demonstrating a covalent association between the two proteins on the surface of the PDA cells.

The formation of a complex between CXCL12 and only KRT19 suggested that this epithelial cell protein serves as an obligatory acceptor for CXCL12. We assessed this hypothesis by CRISPR/Cas9-editing the *Krt19* gene in the mouse PDA line and forming subcutaneous tumors with the edited PDA cells (Fig. 2A; Fig. S2A). The *Krt19*-edited PDA cells, which were identified by their expression of KRT20, lacked the CXCL12-coat (Fig. 2B; Fig. S2B). The tumors also did not exclude T cells (Fig. 2B; Fig. S3A) and grew more slowly than the tumors formed with control PDA cells (Fig. 2C). The activation of the infiltrating T cells was inferred by their increased expression of the effector genes, IFN-γ, perforin and granzyme A (Fig. 2D; Fig. S3B). When subcutaneous tumors were formed with *Krt19*-edited PDA cells in which KRT19 expression had been rescued, both the assembly of the CXCL12-coat and the exclusion of T cells were again observed (Fig. S4).

The stability of the CXCL12-KRT19 complex in the presence of SDS suggested a covalent linkage between the two proteins. TGM2 forms inter-molecular, isopeptide bonds between glutamines and the γ-amino groups of lysines (*17*), and is expressed by epithelial cells and myelomonocytic cells. We anticipated that cancer cell-derived TGM2 would be the relevant source of this enzyme because the presence of infiltrating myelomonocytic cells would be mutually exclusive with the formation of the CXCL12-coat. Therefore, we CRISPR/Cas9-edited *Tgm2* in PDA cancer cells and induced subcutaneous tumors with the modified cells (Fig. 3A; Fig. S5). In some areas of these tumors, the TGM2-deficient PDA cancer cells lacked CXCL12-staining, whilst in other areas, cancer cells had CXCL12-staining, but this was significantly less than that of cancer cells expressing TGM2 (Fig. 3A-D). Therefore, the absence of TGM2-expression in PDA cells alters the fixed, stoichiometric relationship between KRT19 and CXCL12 that is observed in the tumors formed with unedited PDA cells. This less effective CXCL12-coating of *Tgm2*-edited cancer cells, which may reflect the activity of TGM2 from infiltrating myelomonocytic cells, however, was not sufficient to prevent the intra-tumoral accumulation of activated T cells when we quantified the T cell number and gene expression in CXCL12-low and CXCL12-negative areas (Fig. 3E, F; Fig S6). Furthermore, the T cell density in these two areas of the *Tgm2*-edited tumors was similar to that of the KRT19-deficient PDA tumors (Fig. 3F). The observation that the *Tgm2*-edited PDA tumors and *Krt19*-edited PDA tumors have similar T cell infiltration and slower growth rates (Fig. 3G) suggests that only the CXCL12-coat assembled by TGM2 expressed by the PDA cell has an immune modulatory effect.

We determined whether the presence of the CXCL12-coat on PDA cancer cells was the basis for the resistance of PDA tumors to antagonists of the PD-1 checkpoint. Mice with established, subcutaneous tumors formed with non-edited PDA cells, *Krt19*-edited PDA cells, and *Tgm2*-edited PDA cells, respectively, were treated with control IgG or anti-PD-1 antibody for one week, avoiding the confounding effects of neutralizing anti-rat antibodies (Fig. S7). Anti-PD-1 antibody treatment caused regression of tumors containing either *Krt19*- or *Tgm2*-edited PDA cells (Fig. 4A), but had no effect on control tumors composed of PDA cells having the CXCL12-coat. This heightened intra-tumoral immune reaction occurring when anti-PD-1 was combined with cancer cells lacking the CXCL12-coat is also demonstrated by the enhanced expression of genes indicating the accumulation of activated $CD8^+$ T cells (Fig. S8A). The increased *Cxcl12*

mRNA in these tumors may be an adaptive response of the CAF to this intensified immune reaction (Fig. S8B).

Treatment of hepatic metastasis presents the main therapeutic challenge in the management of patients with PDA. To model this clinical condition, we injected control and *Krt19*-edited, luciferase-expressing PDA cells into the portal veins of mice. The KRT20$^+$ PDA cells in metastatic lesions containing control PDA cells exhibited CXCL12-coats and excluded T cells, as previously shown (*18*). In contrast, *Krt19*-edited PDA cells in metastatic lesions lacked the CXCL12-coat, and cancer cell nests were infiltrated with T cells (Fig. S9A, B). Both types of metastases contained CAFs co-expressing *Cxcl12* and *Pdgfa* (Fig. S9C, D). The infiltrating CD8$^+$ T cells in metastases containing KRT19-deficient cancer cells had elevated mRNA levels of *Ifng, Gzma,* and *Prf1* (Fig. S10A), to which the increased expression of *Cxcl9*, *Cxcl10* and *Cxcr3* may have contributed (Fig. S10B). Intra-tumoral T cell proliferation also occurred, as suggested by the finding of Ki67-expressing CD8$^+$ T cells (Fig. S11). The mRNA levels of the CAF markers, FAP and CXCL12, were not decreased (Fig. S10B), constituting further evidence that the availability of CXCL12 was not a contributing factor to the absence of the CXCL12-coat on the KRT19-deficient PDA cells. Finally, and most importantly, treatment of mice with anti-PD-1 prevented the growth of hepatic metastases formed with PDA cells lacking KRT19 and the CXCL12-coat. Metastases containing control PDA cells having the CXCL12-coat did not respond to this immunotherapy (Fig. 4B; Fig. S12).

These studies demonstrate that the intra-tumoral accumulation of T cells is regulated by the capacity of cancer cells to capture CXCL12 from the tumor microenvironment. The cancer cell component of this response depends on the expression of KRT19 and TGM2. The translational relevance of these experiments is demonstrated by finding the CXCL12-coat on multiple human carcinomas, and by the reduced survival of patients with pancreatic cancer and high intra-tumoral KRT19 or TGM2 expression (Fig. S13). It is probable that this biochemical coating mechanism evolved to protect normal epithelial cells from immune attack by appropriating the immune suppressive effects of CXCL12, a product of a fibroblastic cell type that resides in normal tissues (*19*) and accumulates in inflammatory lesions (*20*). The critical cellular event may be the coordinated secretion of KRT19 and TGM2 by an unconventional pathway, which is necessitated by the absence in both proteins of a signal peptide. Although the extracellular secretion of these proteins has been demonstrated (*21, 22*), the stimulus has not been identified. We also have not explained how cancer cell-associated CXCL12 suppresses the intra-tumoral trafficking of T cells, but the mechanism must involve its receptor, CXCR4 (*13*), and may relate to the reported capacity of high concentration CXCL12 to cause chemorepulsion of T cells *in vitro* (*23*). The current study identifies TGM2 as a potential combination therapy target in immunotherapy trials, but it particularly emphasizes the urgent need to assess the combined therapeutic efficacy of CXCR4 inhibitors with blockade of the PD-1/PDL1 axis in patients with PDA.

References and Notes:

1. J. A. Joyce, D. T. Fearon, *Science* **348**, 74-80 (2015).

2. J. Galon *et al.*, *Science* **313**, 1960-1964 (2006).
3. A. Snyder *et al.*, *N Engl J Med* **371**, 2189-2199 (2014).
4. N. A. Rizvi *et al.*, *Science* **348**, 124-128 (2015).
5. E. M. Van Allen *et al.*, *Science* **350**, 207-211 (2015).
6. M. Platten, W. Wick, B. J. Van den Eynde, *Cancer Res* **72**, 5435-5440 (2012).
7. S. Mariathasan *et al.*, *Nature* **554**, 544-548 (2018).
8. L. M. McLane, M. S. Abdel-Hakeem, E. J. Wherry, *Annu Rev Immunol* **37**, 457-495 (2019).
9. S. Z. Josefowicz, L. F. Lu, A. Y. Rudensky, *Annu Rev Immunol* **30**, 531-564 (2012).
10. J. W. Griffith, C. L. Sokol, A. D. Luster, *Annu Rev Immunol* **32**, 659-702 (2014).
11. A. Orimo *et al.*, *Cell* **121**, 335-348 (2005).
12. D. Ohlund *et al.*, *J Exp Med* **214**, 579-596 (2017).
13. C. Feig *et al.*, *Proc Natl Acad Sci U S A* **110**, 20212-20217 (2013).
14. Y. D. Seo *et al.*, *Clin Cancer Res* **25**, 3934-3945 (2019).
15. J. R. Brahmer *et al.*, *N Engl J Med* **366**, 2455-2465 (2012).
16. S. L. Topalian *et al.*, *N Engl J Med* **366**, 2443-2454 (2012).
17. S. Gundemir, G. Colak, J. Tucholski, G. V. Johnson, *Biochim Biophys Acta* **1823**, 406-419 (2012).
18. A. Pommier *et al.*, *Science* **360**, (2018).
19. E. W. Roberts *et al.*, *J Exp Med* **210**, 1137-1151 (2013).
20. A. P. Croft *et al.*, *Nature* **570**, 246-251 (2019).
21. C. Alix-Panabieres *et al.*, *Breast Cancer Res* **11**, R39 (2009).
22. M. Adamczyk, R. Griffiths, S. Dewitt, V. Knauper, D. Aeschlimann, *J Cell Sci* **128**, 4615-4628 (2015).
23. M. C. Poznansky *et al.*, *Nat Med* **6**, 543-548 (2000).

Acknowledgments: We thank Dr. David Tuveson for providing the 1242 PDA cells. We also acknowledge the contributions of the Cold Spring Harbor Laboratory facilities of Animal, Microscopy, Flow Cytometry, and Animal Imaging. **Funding:** This study was supported by the Distinguished Scholar Award of the Lustgarten Foundation (D.T.F.), the Thompson Family Foundation (D.T.F.), the Cedar Hill Foundation (D.T.F.), and the National Cancer Institute (D.T.F. and T.J.). **Author contributions:** D.T.F. and Z.W. conceived the project. Z.W., J.L. and Y.G. performed the experiments; D.T.F., T.J., Z.W., J.L. and Y.G. analyzed data; D.T.F. and Z.W. wrote the manuscript; D.T.F., T.J., Z.W. and Y.G. revised the manuscript. **Conflict of Interest:** The authors disclose no potential conflicts of interest.

Supplementary Materials:

Materials and Methods

Figures S1-S13

Tables S1-S2

References (*24-25*)

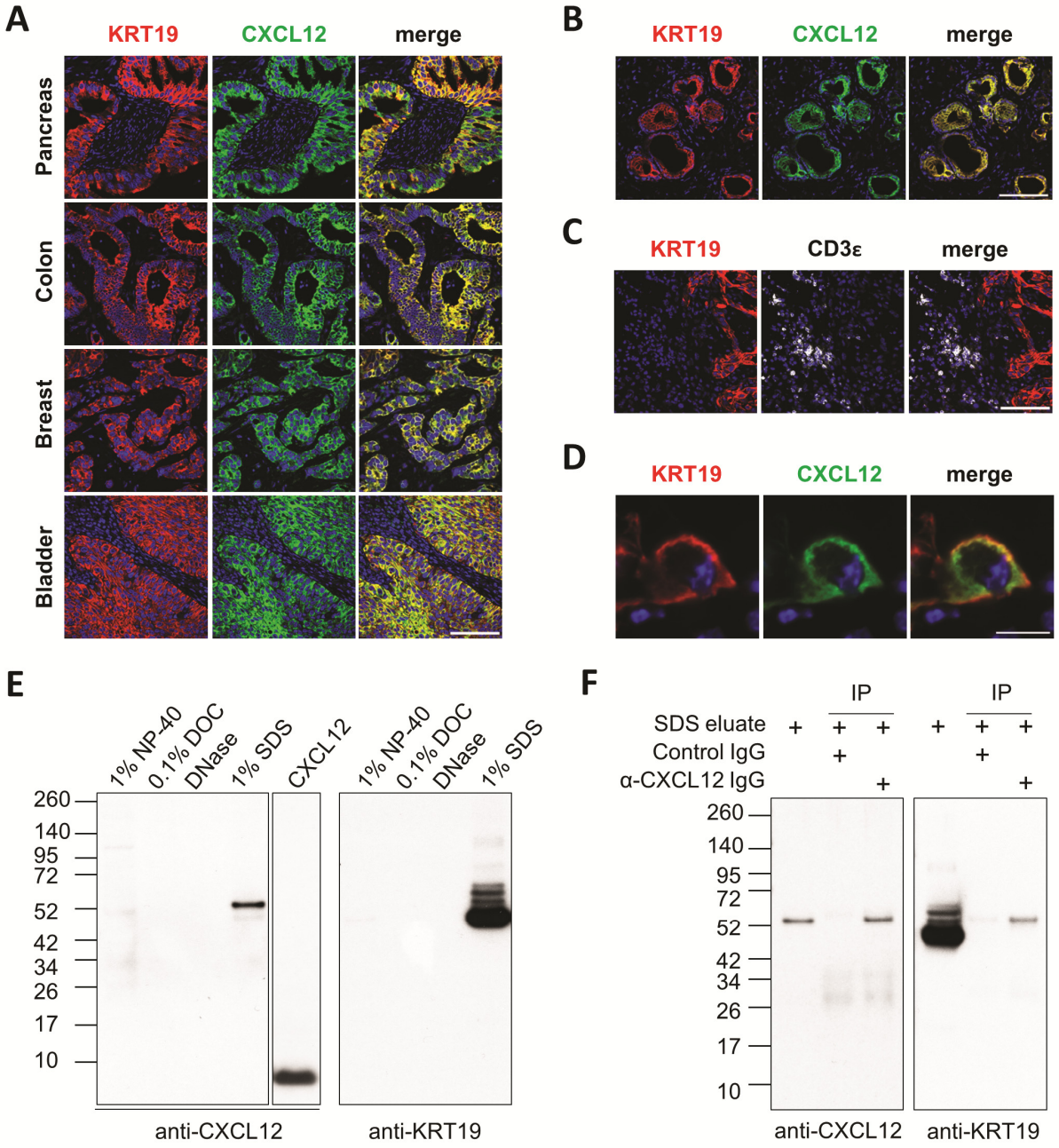

Figure 1: The CXCL12-coat of cancer cells in human and mouse adenocarcinomas. (**A-D**) Sections of human adenocarcinomas (A), mouse autochthonous PDA (B) and subcutaneous PDAs (C, D), were stained with fluorescent antibodies to KRT19 (A-D) to reveal cancer cells, and to CXCL12 (A, B and D) and CD3ε (C). (**E**) Sequential detergent eluates of a subcutaneous PDA tumor and recombinant CXCL12 were subjected to SDS-PAGE and immunoblotting with anti-KRT19 or anti-CXCL12. (**F**) The SDS-eluate from a subcutaneous PDA tumor and the proteins immunoprecipitated with control IgG or anti-CXCL12 were subjected to SDS-PAGE and immunoblotting with anti-KRT19 and anti-CXCL12. Scale bars, 100 µm (A-C), 10 µm (D).

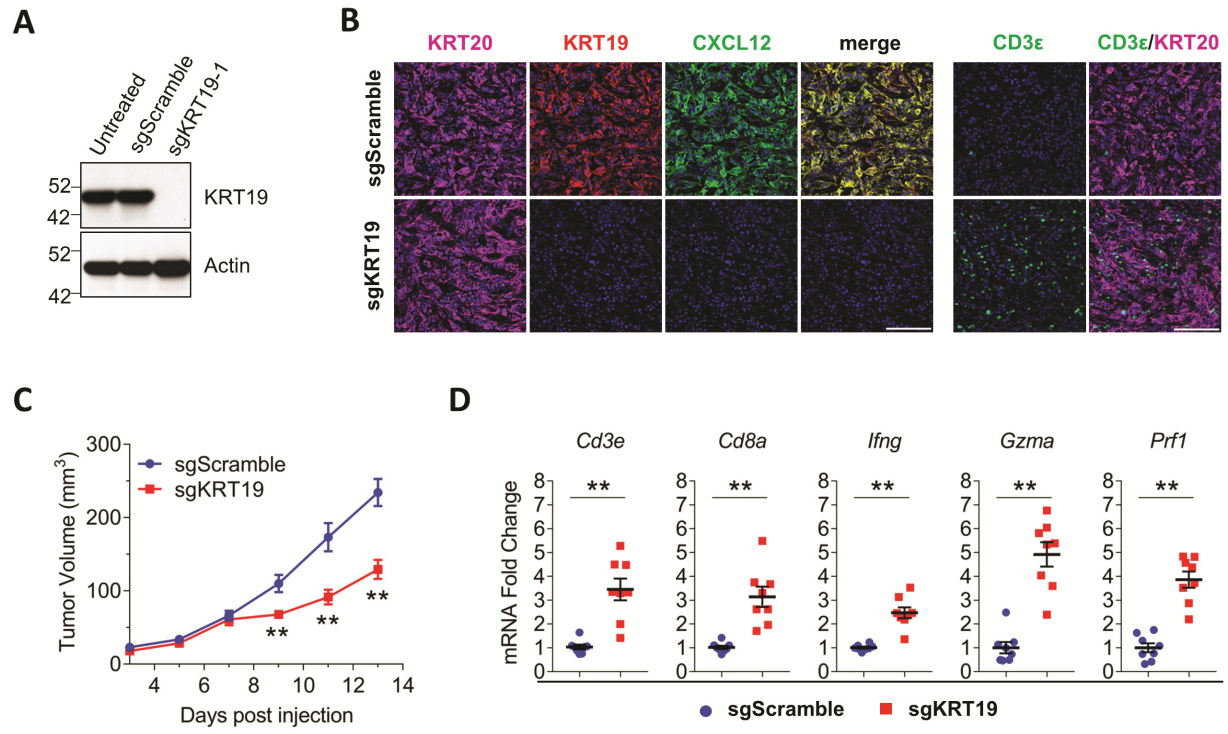

Figure 2: The role of KRT19 expression by mouse PDA cells in CXCL12-coat formation and tumor T cell infiltration. (**A**) Lysates of mouse PDA cell lines that were untreated or CRISPR/Cas9 edited with different guide RNAs (sg) were subjected to SDS-PAGE and immunoblotting with anti-KRT19 and anti-actin. (**B**) Sections of subcutaneous tumors formed with sgScramble control PDA cells and the *Krt19*-edited PDA cells, respectively, were stained with fluorescent antibodies to KRT20 to reveal cancer cells, KRT19, CXCL12, and CD3ε, respectively. Scale bars, 100 µm. (**C**) The growth curves of subcutaneous tumors formed with the control and *Krt19*-edited PDA cells are displayed (n=8 per group). Mean ± SEM; ** $p<0.01$, Multiple Student's *t*-test. (**D**) The mRNA levels for immune genes were measured in PDA tumors taken from mice 13 days after initial subcutaneous inoculation of the control and *Krt19*-edited PDA cells. Mean ± SEM; ** $p<0.01$, Student's *t*-test.

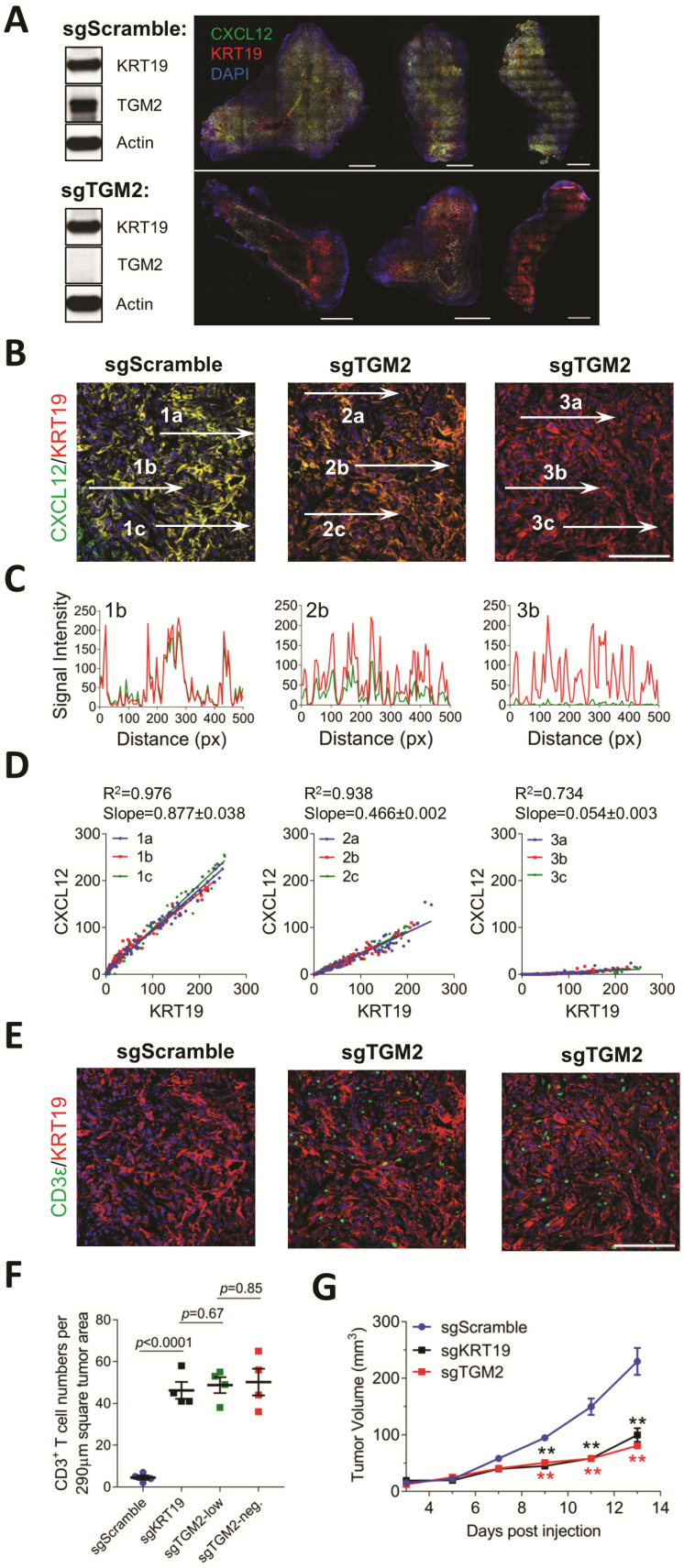
A
sgScramble:
KRT19
TGM2
Actin
sgTGM2:
KRT19
TGM2
Actin
CXCL12
KRT19
DAPI
B
sgScramble
sgTGM2
sgTGM2
CXCL12/KRT19
1a
1b
1c
2a
2b
2c
3a
3b
3c
C
Signal Intensity
1b
2b
3b
Distance (px)
D
R²=0.976
Slope=0.877±0.038
R²=0.938
Slope=0.466±0.002
R²=0.734
Slope=0.054±0.003
CXCL12
KRT19
E
sgScramble
sgTGM2
sgTGM2
CD3ε/KRT19
F
CD3⁺ T cell numbers per 290μm square tumor area
p<0.0001
p=0.67
p=0.85
sgScramble
sgKRT19
sgTGM2-low
sgTGM2-neg.
G
Tumor Volume (mm³)
sgScramble
sgKRT19
sgTGM2
Days post injection

Figure 3: The role of TGM2 expression by mouse PDA cells in CXCL12-coat formation, T cell infiltration, and tumor growth. (A) Lysates of mouse PDA cell lines that were untreated or CRISPR/Cas9 edited with different guide RNAs were subjected to SDS-PAGE and immunoblotting with anti-KRT19, anti-TGM2 and anti-actin antibodies. Tumors formed with these PDA cell lines were stained with fluorescent anti-KRT19 and anti-CXCL12 antibodies. Representative fluorescent images of entire cross sections of three tumors of each type are shown, demonstrating high CXCL12 staining of all KRT19-positive, sgScramble PDA cells, and absent or low CXCL12-staining of KRT19-positive sgTGM2 PDA cells. Scale bars, 1 mm. (**B-D**) The three regions of the two PDA tumor types were assessed for signal intensities of anti-KRT19 and anti-CXCL12 staining by horizontal line scans of 500 pixels (B, C). Scatter plots for all pixels of the horizontal line scans are displayed to assess the correlation between the CXCL12 and KRT19 staining intensities. The R^2 values and slopes (Mean ± SEM) are shown (D). Scale bar, 100 µm. (**E, F**) The three regions of the two tumor types were also assessed for infiltrating T cells by staining with anti-CD3ε antibody. Scale bar, 100 µm. (**G**) The rates of growth of subcutaneous tumors formed with sgScramble PDA cells, sgKRT19 PDA cells, and sgTGM2 PDA cells, respectively, are shown. Mean ± SEM; **$p<0.01$, Multiple Student's *t*-test.

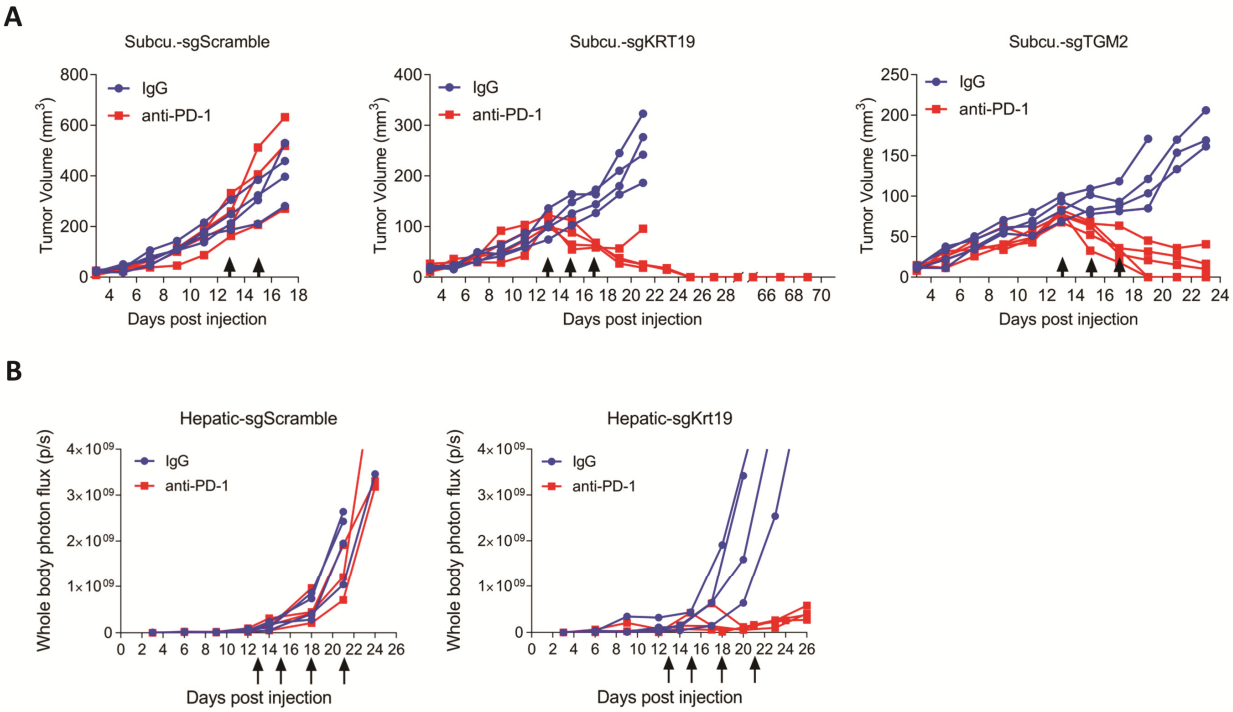

Figure 4: Sensitivity of PDA tumors with cancer cells lacking the CXCL12-coat to treatment with anti-PD-1. (**A**) Mice bearing subcutaneous tumors formed with the control or CRISPR/Cas9-edited PDA cells lacking expression of KRT19 or TGM2 were treated by intra-peritoneal administration of non-immune IgG or anti-PD-1 (arrows), and tumor growth was measured. (**B**) Mice bearing hepatic metastases formed with luciferase-expressing CRISPR/Cas9-edited PDA cells were treated by intra-peritoneal administration of non-immune IgG or anti-PD-1 (arrows), and metastasis growth was measured by bioluminescent imaging.

Supplementary Materials

Materials and Methods

Human Tumor Arrays

Formalin fixed paraffin embedded (FFPE) human tumor arrays for pancreas cancer (PA501a), colon cancer (BC05021a), breast cancer (BC08013c), bladder cancer (BC12011d), melanoma (ME483a) and frozen multiple organ tumor/tissue arrays (FMC282e and FMO401) were purchased from US Biomax.

Animals

Male C57Bl/6 mice of 6 weeks old were purchased from The Jackson Laboratory. After receiving, the mice were housed in helicobacter free room for 2 weeks before experiment. All experimental procedures conducted on mouse were approved by the Cold Spring Harbor Laboratory (CSHL) Institutional Animal Care and Use Committee (IACUC). And the NIH "Guide for the Care and Use of Laboratory Animals" was complied with in animal studies.

CRISPR editing and lentivirus

The control CRISPR guide (sgScramble: GCTTAGTTACGCGTGGACGA (*24*)) and the guides targeting to mouse *Krt19* gene (sgKRT19-1: CACAGGAAATTACTGCCCTG; sgKRT19-2: TAGTGGTTGTAATCTCGGGA; sgKRT19-3: CGGAGGACGAGGTCACGAAG) or mouse *Tgm2* gene (sgTGM2-1: GAATATGTCCTTACGCAACA; sgTGM2-2: GTCCTGTTGGTCCAGCACTG; sgTGM2-3: TTGACCTCGGCAAACACGAA) were cloned into the lentiCRISPR-v2 plasmid (Addgene, 52961) and sequencing validated. The lentivirus was produced by co-transfecting HEK293T cells with the guide containing lentiCRISPR-v2 plasmid together with the lentivirus packing plasmid psPAX2 (Addgene, 12260) and the envelop expressing plasmid pMD2.G (Addgene, 12259).

Cell Lines

Mouse pancreas ductal adenocarcinoma (PDA) cancer cell line 1242 which was derived from KPC (LSL-Kras$^{G12D/+}$; LSL-Trp53$^{R172H/+}$; Pdx1-Cre) mouse tumor (*25*) is a gift from D. Tuveson lab. To generate sgScramble, sgKRT19 and sgTGM2 cell lines, 1242 cells were transduced with lentivirus expressing SpCas9 and specific CRISPR guide. The transduced cells were directly selected with 1 μg/ml puromycin (Sigma, P8833) for polyclonal stable cell lines. The single cell clones were generated by limited dilution. Most experiments were done with the single cell clones otherwise indicated. To rescue KRT19 expression in the *Krt19*-edited cancer cells which was achieved by transduction with the lentivirus containing the sgKRT19-1 guide, the single cell clone was further transduced with lentivirus expressing mouse KRT19 with four synonymous mutations at the guide targeting site (Fig. S4A). To facilitate tumor imaging *in vivo* for hepatic metastasis, the sgScramble and sgKRT19 cell lines were further introduced with lentiviral plasmid expressing firefly luciferase and GFP which are linked by 2A peptide. The luciferase/GFP transduced cells were sorted by FACS. All the cell lines were cultured in DMEM medium (Cellgro, 10-013-CV) supplemented with 10% FBS (Seradigm, 1500-500), 100 units/ml penicillin and 100 μg/ml streptomycin.

Mouse studies

For subcutaneous tumors, 2.5×10^5 cells, or otherwise indicated, were injected at right flank of mouse. Tumor volume was measured with caliper every two days and calculated according to the formula $V = (L\times W^2)/2$. Mice developed with tumor associated ulcer before end of the experiment were ruled out, and the ulcerated tumors were not included in any analysis. For hepatic metastasis model, 2.5×10^4 or 1.0×10^5 luciferase expressing cells were injected through portal vein. Tumor size was monitored through bioluminescence imaging every 3 or 4 days. Basically, 150 µl of 30 mg/ml D-Luciferin (Perkin-Elmer, 122799-10) was administered through intraperitoneal injection and mice were imaged with the IVIS Spectrum *in vivo* Imaging System. For tumor treatment, 200 µg isotype IgG (BioXcell, BP0089) or Rat anti-mouse PD-1 antibody (BioXcell, BP0273) was given through intraperitoneal injection on indicated days. T cell depletion was done by intraperitoneal injection of 200 µg anti-CD4 (BioXcell, BP0003) and anti-CD8 (BioXcell, BP0061) antibodies twice a week.

Immunofluorescence

Mouse tumors were embedded in Tissue-Tek OCT compound (Sakura, 4583) and freshly frozen on dry ice. In the case of hepatic metastatic tumors, the whole livers were perfused through portal vein with cold PBS before freezing. The embedded tumors were sectioned at 10µm for staining. For Human FFPE tumor arrays, the slides were deparaffinized in Xylene for three times (5 min each) followed by sequential rehydration treatments in 100% ethanol (5 min, 3 times), 95% ethanol (10 min, twice), 70% ethanol (10 min, twice), 50% ethanol (10 min, twice), and water (5 min, twice). After rehydration, antigen retrieval was conducted by boiling the sample in 10mM Tris-HCl (pH 8.8) plus 1mM EDTA for 10 min. Then, keep the sample slides in the boiled buffer and cool down on bench top for 30 min followed by wash in water for 5 min, twice.

To stain tumor sections, the samples were fixed with freshly prepared PLP buffer (100 mM phosphate buffer, pH 7.4, 80 mM L-lysin, 10 mM $NaIO_4$, and 4% paraformaldehyde) for 10 min at room temperature. After wash with PBS, hydrophobic barrier was drawn around the tumor slice with ImmEdge PAP pen (Vector Laboratories, H-4000). The sections were then permeabilized with 0.2% TritonX-100 in PBS for 15 min followed by blocking with 1% BSA (Calbiochem, 2930) plus 10% normal goat serum (Thermo, 16210064) in PBS for 1 hour at room temperature. Non-conjugated primary antibodies (Table S1) were incubated at 4°C overnight. Fluorophore conjugated secondary antibodies were incubated at room temperature for 1 hour. And fluorophore conjugated primary antibodies (Table S1) were incubated at room temperature for 2 hours. Nuclei were stained with DAPI (Thermo, R37606) at room temperature for 10min. In between each steps, sections were washed with 0.05% Tween-20 in PBS for 5min twice and PBS for 5 min once. Afterwards, tumor sections were mounted with mounting medium (Thermo, P36961). For the staining of the thick (30 µm) non-permeabilized section (Fig. 1C), TritonX-100 was not included. Images were acquired on Leica SP8 confocal microscope or ZEISS Observer microscope and analyzed with ImageJ software.

Tumor Protein Extraction

Tumor pieces of about 100 mg were used for protein extraction. Freshly dissected tumor piece or the tumor piece that was previously flash-frozen in liquid nitrogen and stored in -80°C was homogenized in 1 ml ice cold IP buffer (75 mM HEPES, pH 7.5, 150 mM NaCl, 1 mM DTT, 10% Glycerol, protease inhibitor cocktail (Thermo, 78437)) plus 1% NP-40. After removal of remaining tissue particles by flowing through the Pierce Tissue Strainer (Thermo, 87791), the

homogenized tissue was sequentially extracted: (1) Re-suspend and incubate at 4°C on rotator for 10min followed by centrifugation at 4,000g for 5 min. Save the supernatant as "NP-40 extract". Repeat to wash the pellet; (2) Re-suspend the pellet in 250 µl IP buffer plus 0.1% sodium deoxycholate (DOC) and incubate at 4°C on rotator for 30 min followed by centrifugation at 6,000g for 5 min. Save the supernatant as "DOC extract". Repeat to wash the pellet; (3) Re-suspend the pellet in 200 µl IP buffer plus 5 mM Ca_2Cl and 3,000 units/ml micrococcal nuclease (Thermo, 88216) and incubate at room temperature for 30 min followed by centrifugation at 16,000g for 5 min. Save the supernatant as "DNase extract". Repeat to wash the pellet; (4) Re-suspend the pellet in 150 µl IP buffer plus 1% SDS and incubate at room temperature for 10 min followed by centrifugation at 16,000g for 5 min. Keep the supernatant as "SDS extract". Protein concentration was measured with protein assay kit (BioRad, 5000112) and 1 µg of each fraction that was boiled in Laemmli sample buffer was applied to SDS-PAGE gel for western blot. The KRT19 antibody TROMA-III, which was deposited by Kemler R. to Developmental Studies Hybridoma Bank (DSHB), was used for western blot.

Immunoprecipitation

SDS in the cytoskeleton fraction was removed with the Pierce Detergent Removal Spin Column (Thermo, 87777). For immunoprecipitation, 100 µg of the protein extract was diluted in 500 µl IP buffer containing 1% BSA (Calbiochem, 2930). To prevent self-assembly of cytokeratin proteins, 0.1% SDS was added. The mixture was pre-cleared by centrifugation at 16,000g for 10 min and the supernatant was transferred in to a new tube. Then, 5 µg Rabbit isotype IgG (Thermo, 10500C) or Rabbit anti-CXCL12 antibody (LSBio, LS-C48888) was added in to the solution followed by incubation on rotor at 4°C overnight. At the same time, protein G agarose beads (Cell signaling, 37478) were also incubated in IP buffer containing 1% BSA overnight. After overnight incubation, 20 µl pure protein G resins (or 40 µl 50% slurry) were added directly to the protein/IgG solution and incubate for another 2 hours at 4°C. Following 3 times wash with IP buffer containing 0.1% SDS, the resins were boiled in 100 µl Laemmli sample buffer and 10 µl sample was applied to SDS-PAGE gel for western blot where Veriblot for IP detection reagent HRP (Abcam, ab131366) was used.

RNA FISH

RNA FISH was done with fresh frozen tumor samples according to user manual of RNAScope Fluorescent Multiplex Reagent kit (ACDBio, 320850). RNAScope probes for mouse *Cxcl12* (422711), *Pdgfra* (480661-C2), and *Krt19* (402941-C3) were used in this study. Images were acquired on Leica SP8 confocal microscope and analyzed with ImageJ.

Flow Cytometry

Freshly resected tumors were minced and digested in complete DMEM cell culture medium containing 250 µg/ml Collagenase D (Sigma, 11088858001), 50 µg/ml Liberase DL (Sigma, 05466202001) and 20 µg/ml DNase I (Sigma, 10104159001) at 37°C for 45 min, shaking. Following lysis of red blood cells in RBC lysis buffer (155 mM NH4Cl, 12 mM NaHCO3 and 0.1 mM EDTA), cells were flown through 70 µm cell strainer and re-suspend in DMEM medium containing 50 µg/ml DNase I to digest released DNA from RBC cells. After incubation at room temperature for 15 min, the cells were washed and re-suspended in FACS buffer (PBS, 2% FBS and 20 mM HEPES, pH 7.4). For staining, the cells were firstly blocked with Rat anti-mouse CD16/CD32 antibody (BioLegend, 101302) in FACS buffer, shaking at 4°C for 30 min. Then,

fluorophore conjugated antibodies (Table S1) were added and incubated for another 30 min in the dark, followed by two times wash in FACS buffer. Calcein violet 450 AM (Thermo, 65-0854-39) or DAPI (Thermo, R37606) was used for live cell gating. Data was acquired, in the CSHL Flow Cytometry Shared Resource, with BD LSRForsseta cell analyzer equipped with Diva software 6.0 and was further analyzed with FlowJo.

RT-qPCR

Tumor samples of about 30mg were flash-frozen in liquid nitrogen and stored in -80°C. Total RNA was extracted with RNeasy mini kit (Qiagen, 74106) according to the manual. To make the cDNA library, 1 µg total RNA was reverse transcribed with Taqman Reverse Transcription Kit (Thermo, N8080234), using oligo d(T)s. cDNA library was then diluted in 100 µl nuclease free water. For RT-qPCR, 5 µl diluted cDNA library was mixed in 384 well plate with specific Taqman probes (Table S2) and Taqman Universal Master Mix II (Thermo, 4440040) to make 10 µl reaction system. The qPCR were run in QuantStudio 6. All the gene expression values were normalized to *Tbp*.

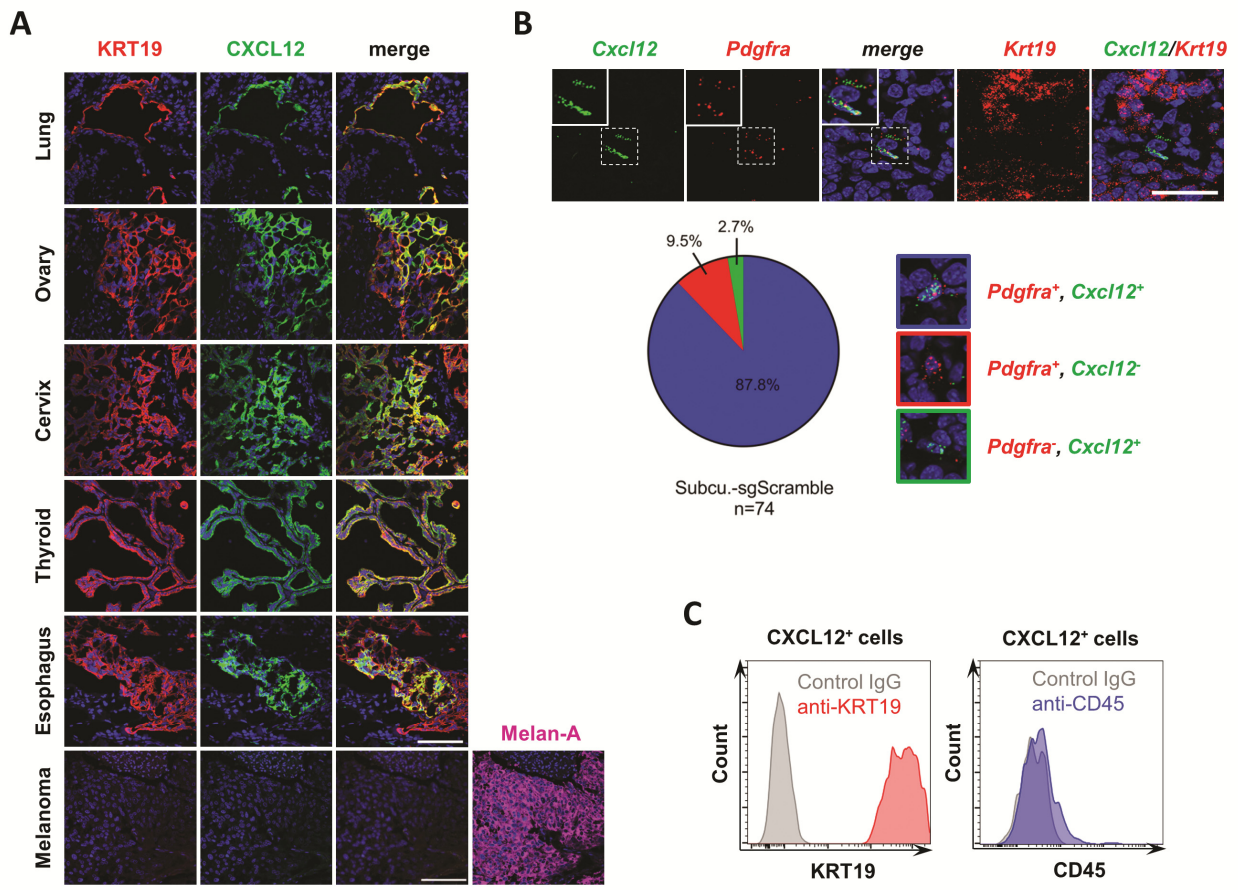

Fig. S1: The characterization of the CXCL12-coat of human and mouse epithelial cancer cells. (**A**) Sections of frozen human carcinomas and formalin-fixed paraffin-embedded (FFPE) human melanoma, were stained with fluorescent antibodies to KRT19 to reveal cancer cells and CXCL12. Scale bars, 100 µm. (**B**) The mRNAs of *Cxcl12, Pdgfra* (fibroblastic stromal cells) and *Krt19* (PDA cells) were detected by RNA FISH in sections of mouse subcutaneous PDA. The pie chart shows relative proportions of the cells that are *Pdgfra*$^{+}$, or *Cxcl12*$^{+}$ or double positive, respectively. Scale bar, 50 µm. (**C**) Intact, dissociated PDA tumor cells were stained with fluorescent antibodies to CXCL12, KRT19 and CD45, and then assessed by FACS.

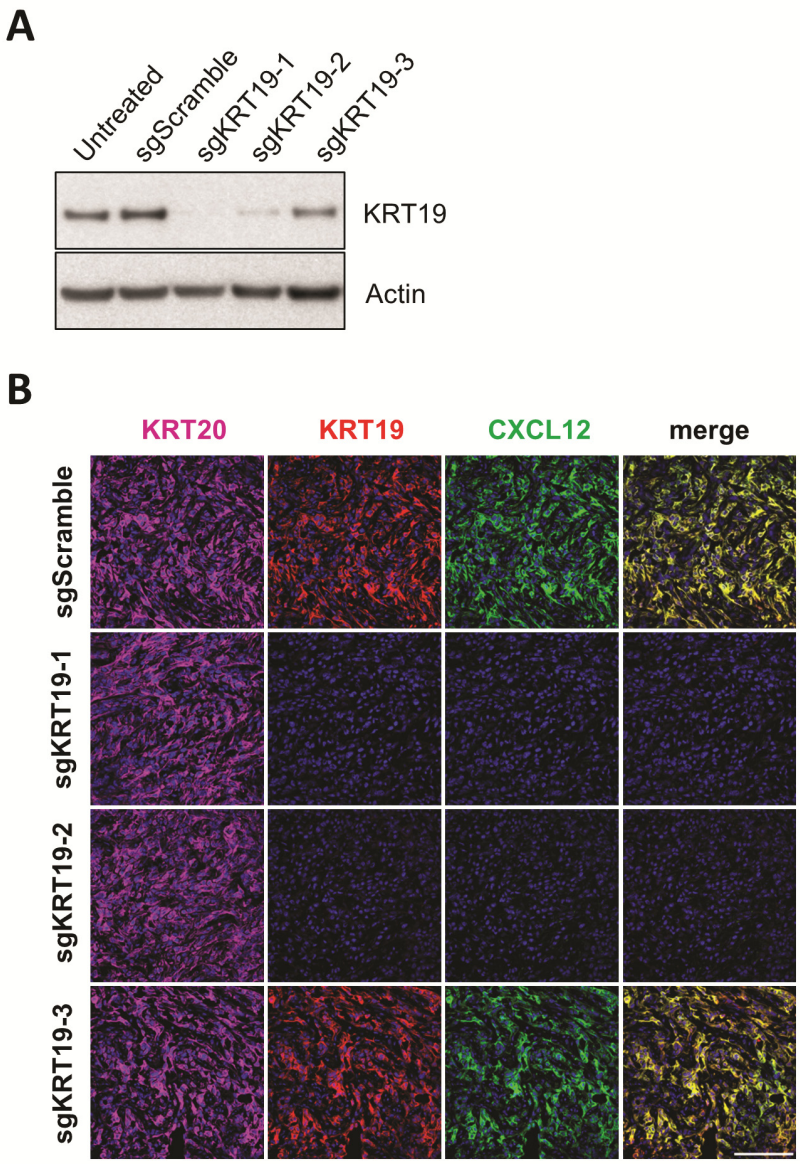

Fig. S2: KRT19 expression by PDA cancer cells and CXCL12 association. (**A**) PDA cells were CRISPR/Cas9 edited using three different KRT19 sgRNAs and assessed for KRT19 expression by SDS-PAGE and immunoblotting with anti-KRT19 antibody. (**B**) Subcutaneous tumors formed with the three *Krt19*-edited PDA lines were stained with fluorescent antibodies to KRT20, KRT19, and CXCL12. The cell lines injected for tumors are polyclonal. Scale bar, 100 μm.

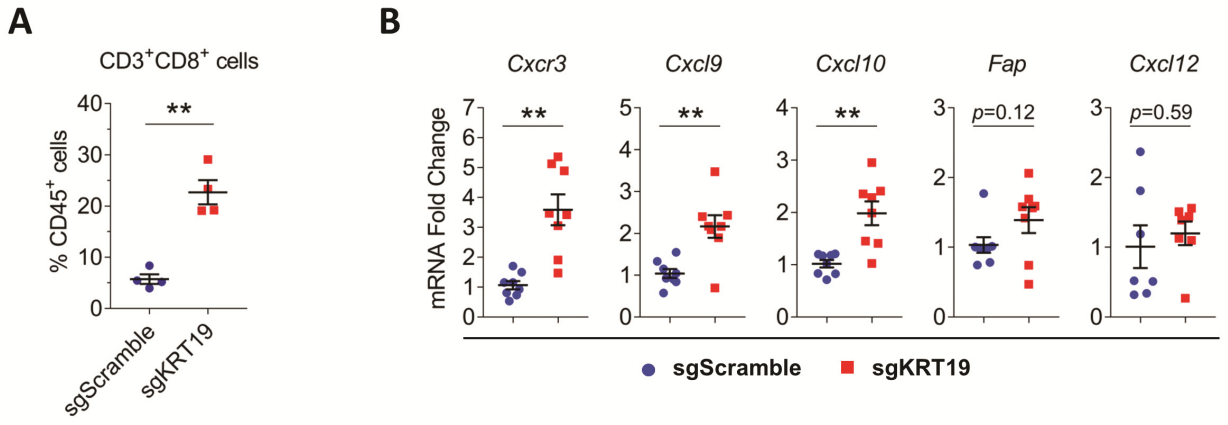

Fig. S3: Analysis of *Krt19*-edited tumors. (**A**) Intact dissociated *Krt19*-edited PDA tumor cells were stained with fluorescent antibodies to CD3, CD8 and assessed by FACS. Mean ± SEM; ** $p<0.01$, Student's *t* test. (**B**) The mRNA levels for genes between the control and the *Krt19*-edited PDA tumors were measured by means of RT-qPCR. The expressions in the control tumors were normalized to 1. Mean ± SEM; ** $p<0.01$, Student's *t* test.

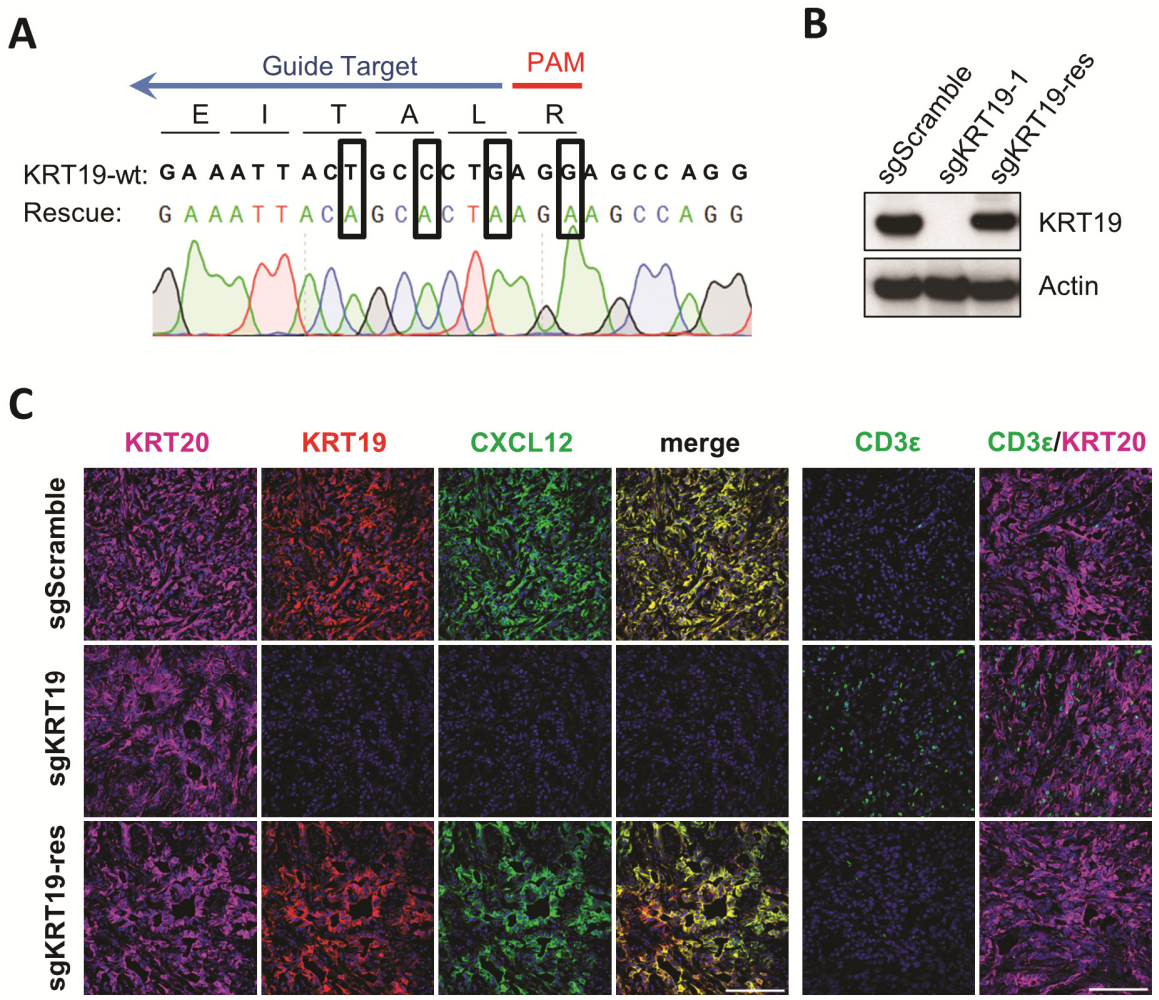

Fig. S4: The rescue the KRT19 expression in *Krt19*-edited PDA cells. (**A**) Sequencing of the KRT19 rescue construct where four synonymous mutations present in black boxes were introduced to prevent the binding of sgKRT19-1. (**B**) PDA cell lysates were subjected to SDS-PAGE and immunoblotting with anti-KRT19. (**C**) Tissue sections of three gene-edited PDA cell lines forming subcutaneous tumors were stained with fluorescent antibodies to KRT20, KRT19, CXCL12, CD3ε, respectively. Scale bars, 100 μm.

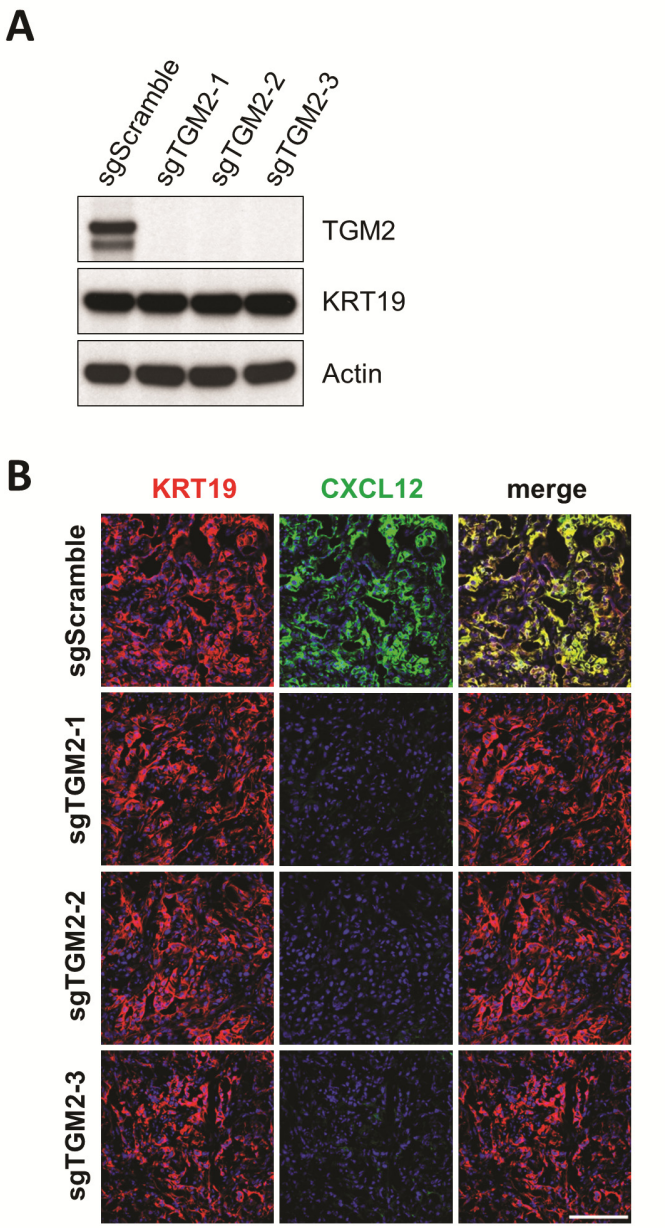

Fig. S5: *Tmg2*-edited PDA cells on the formation of CXCL12-coat. (**A**) Lysates from mouse PDA cell lines that were untreated or CRISPR/Cas9 edited with scrambled sgRNA or three different *Tgm2* sgRNAs were subjected to SDS-PAGE and immunoblotting with anti-TGM2, anti-KRT19 and anti-actin. (**B**) Tissue sections of the control and three *Tgm2*-edited PDA cell lines forming subcutaneous tumors were stained with fluorescent antibodies to KRT19, CXCL12, respectively. The cell lines injected for tumors are polyclonal. Scale bar, 100 μm.

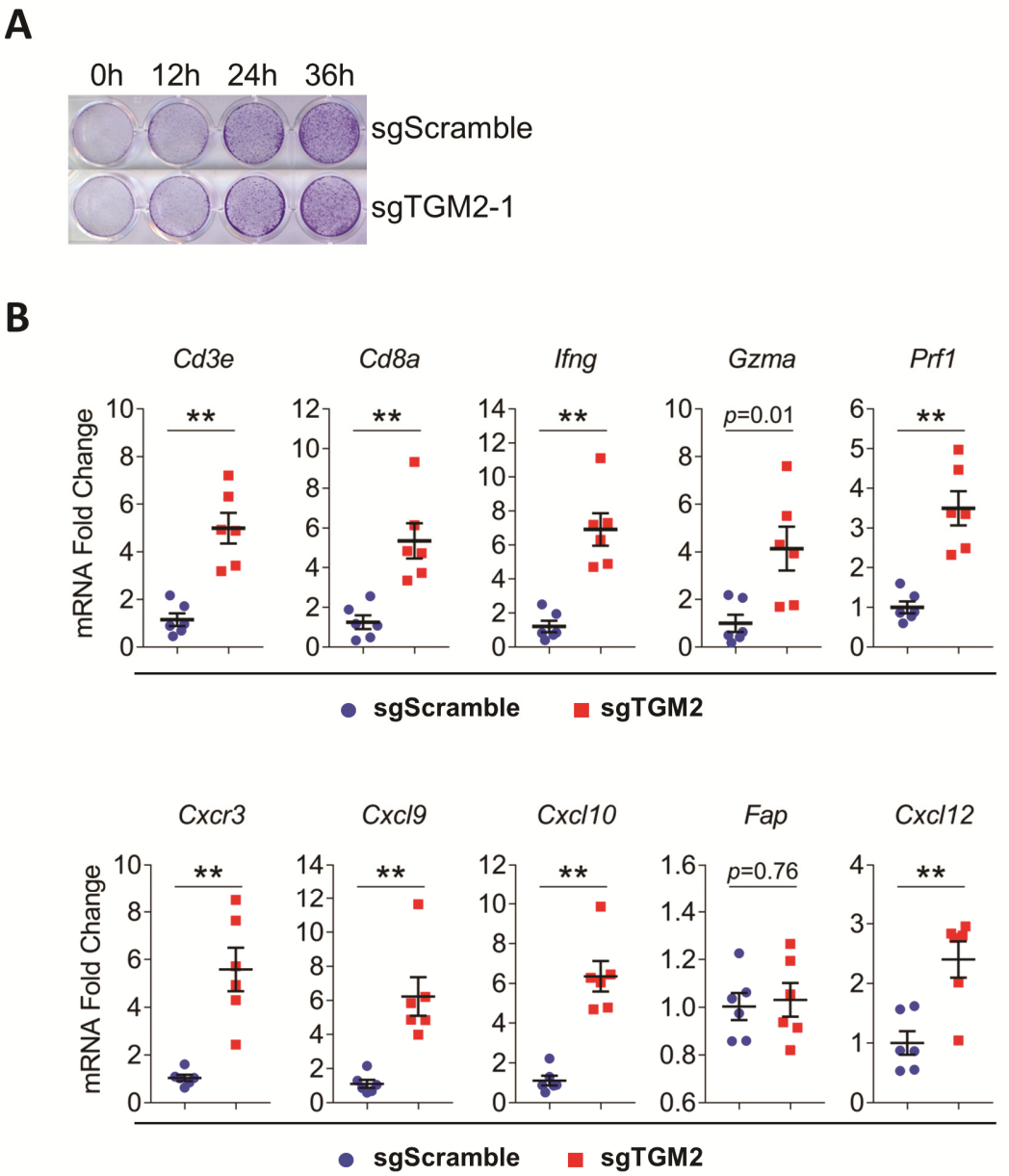

Fig. S6: Characterization of *Tgm2*-edited PDA cells and their tumors. (**A**) In vitro growth of sgScramble and sgTGM2 edited PDA cells are displayed. The same numbers of each cell line were seeded and stained every 12 hours with crystal violet. (**B**) The mRNA levels of immune genes in tumors formed with sgScramble and sgTGM2-1 edited in PDA cells were measured by RT-qPCR. The mRNA levels in sgScramble tumors were normalized to 1. Mean ± SEM; ** $p<0.01$, Student's *t* test.

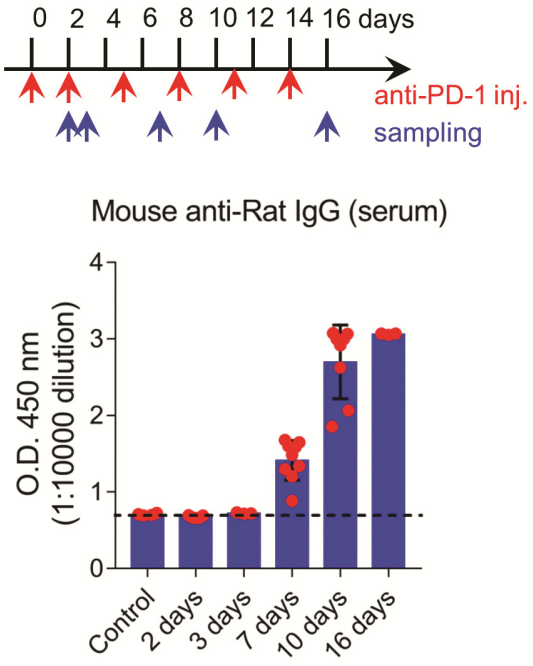

Fig. S7: Development of neutralizing antibody in mice receiving the anti-PD-1 antibody. Mouse anti-rat IgG in blood serum of the mice receiving the anti-PD-1 antibody was measured by means of ELISA. 200 µg anti-PD-1 antibody was administered by intra-peritoneal injections at indicated days (red arrows).

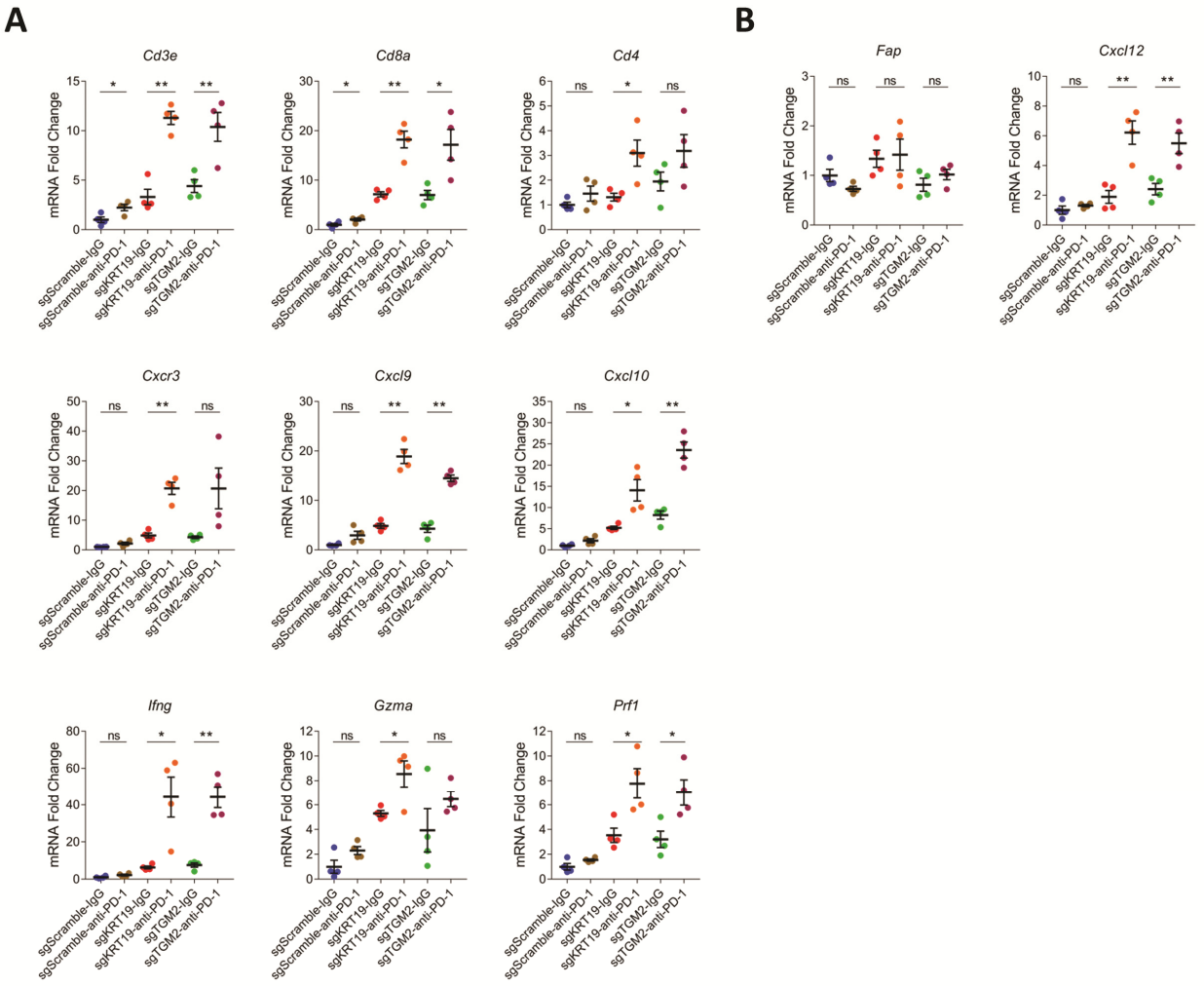

Fig. S8: Gene expression analysis of the subcutaneous PDA tumors treated with anti-PD-1. (**A-B**) The tumor bearing mice were treated with 200 µg isotype IgG or anti-PD-1 antibody at day 13 and day 15 after PDA cancer cell inoculation. Mice were sacrificed at day17, and samples of the tumors were obtained. The mRNA levels of each gene in the tumor samples were measured by means of RT-qPCR. The expression of each gene in sgScramble tumors from mice that had been treated with isotype IgG were normalized to 1. Mean ± SEM; * $p<0.05$, ** $p<0.01$, Student's *t* test.

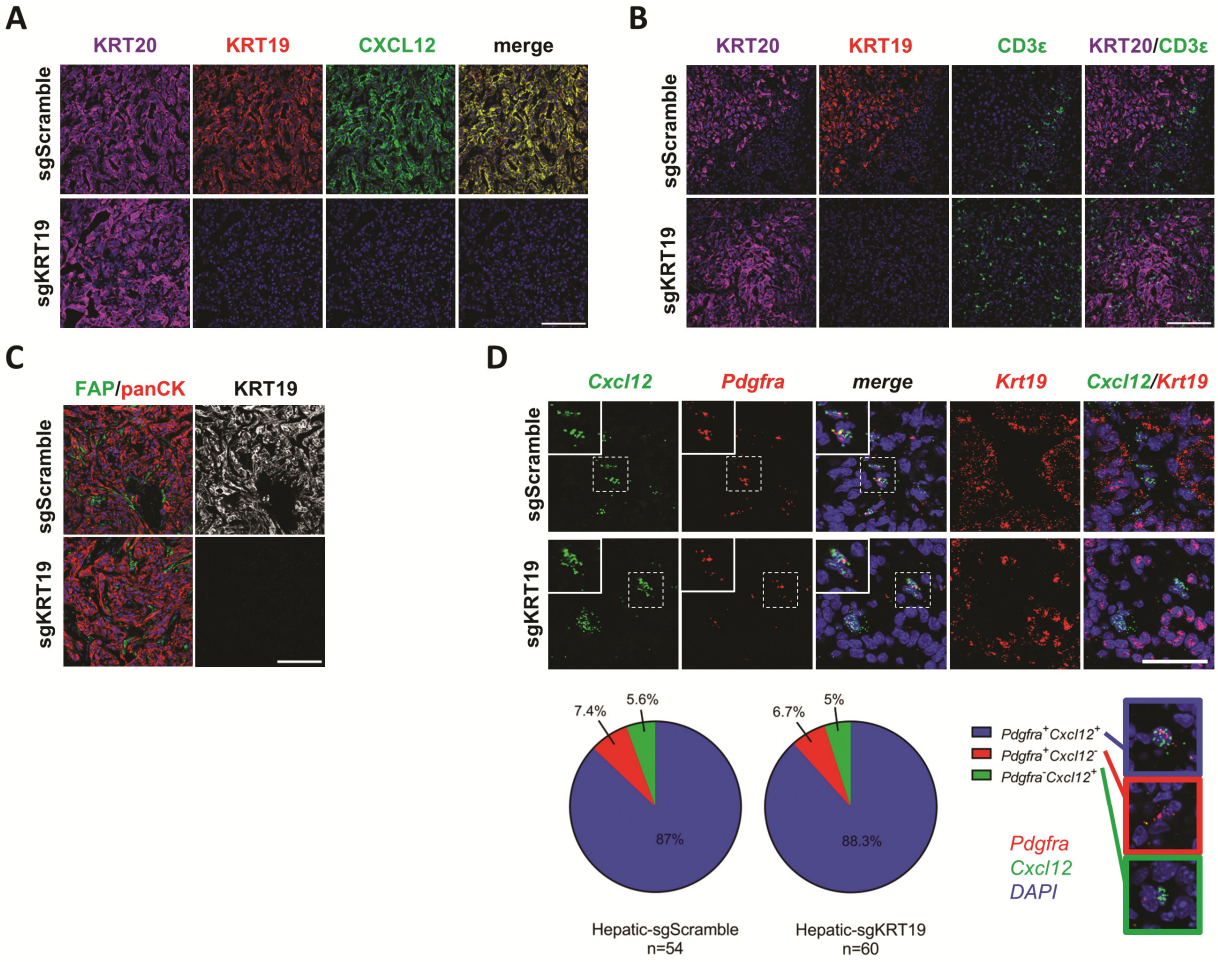

Fig. S9: Characterization of *Krt19*-edited PDA hepatic metastases. (**A-C**) Sections of the control and *Krt19*-edited PDA metastases were stained with fluorescent antibodies to KRT20, KRT19, CXCL12, CD3ε, FAP, panCK, respectively. Scale bars, 100 µm. (**D**) mRNAs for *Cxcl12, Pdgfra* and *Krt19* were detected by RNA FISH in liver metastasis sections. The pie chart shows relative proportions of the cells that are *Pdgfra*$^+$, or *Cxcl12*$^+$ or double positive, respectively. Scale bar, 50 µm.

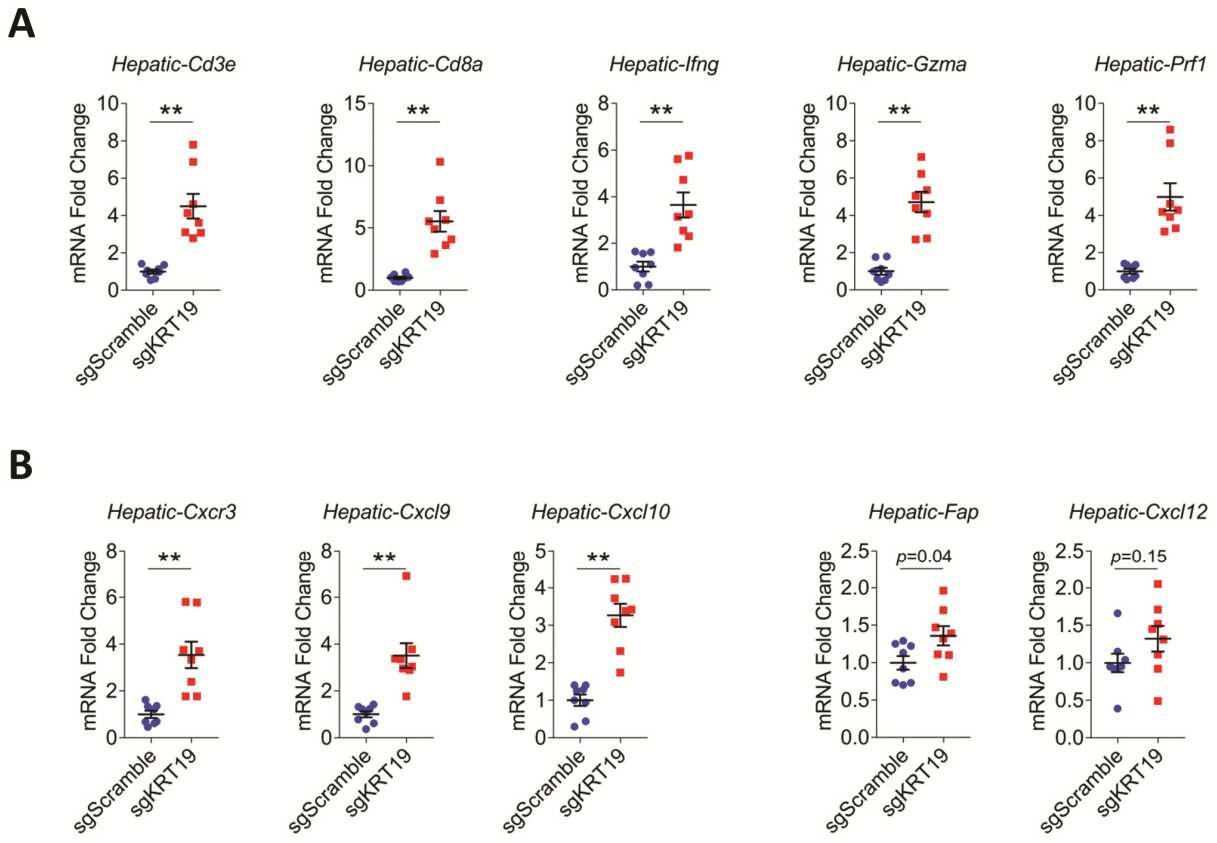

Fig. S10: Expression of immune genes in hepatic metastases formed with control (sgScramble) and *Krt19*-edited (sgKRT19) PDA cells (**A-B**) The mRNA levels were measured by RT-qPCR and expression of each gene were normalized to that of the control 1evels, which were assigned a value of 1. Mean ± SEM; ** $p<0.01$, Student's *t* test.

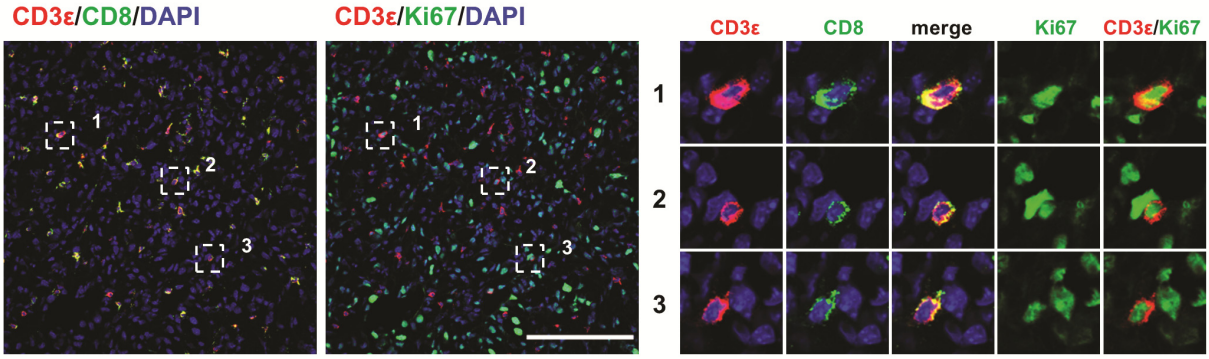

Fig. S11: Analysis of proliferative state of infiltrating CD8$^+$ T cells in *Krt19*-edited hepatic metastases. Sections of the metastases were stained with antibodies to CD3ε, CD8 and Ki67. Scale bar, 100 μm.

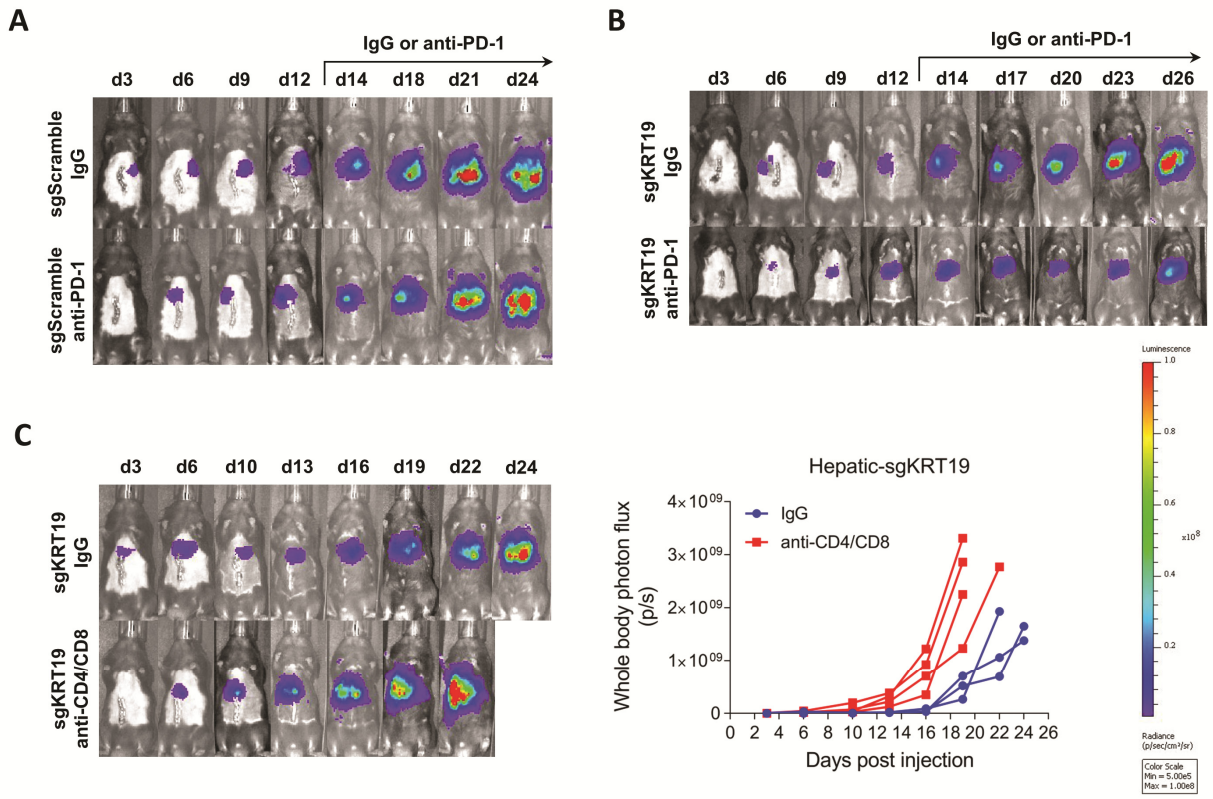

Fig. S12: Bioluminescent images of hepatic metastases formed with luciferase-expressing control and *Krt19*-edited PDA cells. (**A** and **B**) Representative bioluminescence images of the mice in which metastasis growth was depicted in Fig. 4B. (**C**) Hepatic metastases were formed by injecting 2.5×10^4 *Krt19*-edited PDA cells into the portal vein at day 0 in mice that had been pre-treated with non-immune IgG or depleting antibodies to CD4 and CD8, and growth of the metastases was measured by bioluminescent imaging.

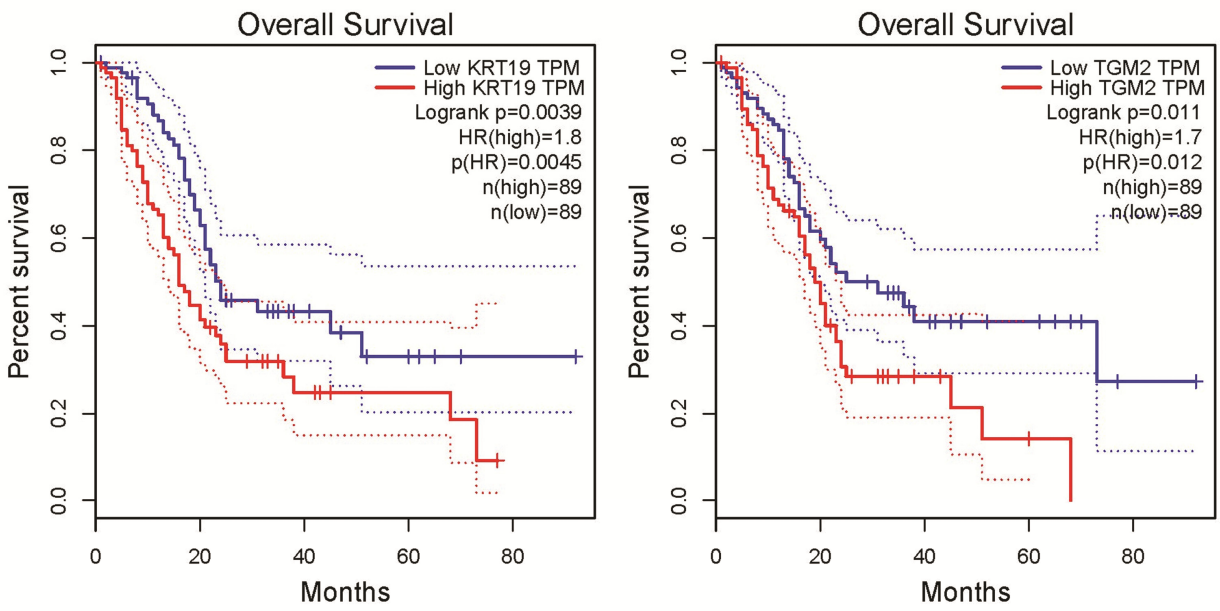

Fig. S13: Kaplan-Meier survival analysis of patients with PDA stratified by KRT19 and TGM2 expression. TCGA data were analyzed. Group cut-offs were set at median expression level for the respective transcript.

Table S1: Primary antibody list

Antibody	Vendor	Catalog NO.	Reactivity	Application
KRT19-AF568	Abcam	ab203445	Hs, Mm	IF, FC
KRT19-AF647	Abcam	ab192980	Hs, Mm	IF, FC
CXCL12-FITC	R&D	IC350F	Hs, Mm	IF (Frozen), FC
Melan-A-AF647	NOVUS	NBP2-46603AF647	Hs	IF
CD45-BV510	BioLegend	103138	Mm	FC
CD3-PE	BioLegend	100206	Mm	FC
CD8-APC/Cy7	BioLegend	100714	Mm	FC
CD3-AF647	BioLegend	100209	Mm	IF
Rb-anti-CXCL12	Peprotech	500-P87A	Hs	IF (FFPE), WB
Rb-anti-CXCL12	LSBio	LS-C48888	Mm	IP
Rt-anti-KRT19	DHSB	TROMA-III	Mm	WB
Rb-anti-KRT20	Abcam	ab230524	Mm	IF
Sh-anti-TGM2	R&D	AF5418	Mm	WB
Rb-anti-Actin	Abcam	ab8227	Mm	WB
Rb-anti-FAP	Millipore	ABT11	Mm	IF
Rb-anti-Ki67	NOVUS	NB110-89717SS	Mm	IF (Frozen)
Rt-anti-CD3	BioLegend	100202	Mm	IF
Rt-anti-CD8	BioLegend	100702	Mm	IF
Rt-anti-CD8	BioXcell	BP0061	Mm	T cell Depletion
Rt-anti-CD4	BioXcell	BP0003	Mm	T cell Depletion
Rt-anti-PD-1	BioXcell	BP0273	Mm	PD-1 blocking

Table S2: Taqman probes for RT-qPCR (Thermo)

Gene	Catalog NO.
Tbp	Mm00446973_m1
Cd3e	Mm00599683_m1
Cd8a	Mm01182107_g1
Ifng	Mm01168134_m1
Gzma	Mm01304452_m1
Prf1	Mm00812512_m1
Cd4	Mm00442754_m1
Cxcr3	Mm00438259_m1
Cxcl9	Mm00434946_m1
Cxcl10	Mm00445235_m1
Fap	Mm00484254_m1
Cxcl12	Mm00445553_m1

References

(24) K. Suzuki *et al.*, In vivo genome editing via CRISPR/Cas9 mediated homology-independent targeted integration. *Nature* **540**, 144-149 (2016).

(25) S. R. Hingorani *et al.*, Trp53R172H and KrasG12D cooperate to promote chromosomal instability and widely metastatic pancreatic ductal adenocarcinoma in mice. *Cancer Cell* **7**, 469-483 (2005).